Railway wheelset fatigue life estimation based on field tests

Received: 12 January 2022 | Revised: 8 May 2022 | Accepted: 25 May 2022

DOI: 10.1111/ffe.13756

ORIGINAL ARTICLE

FFEMS Fatigue & Fracture of Engineering Materials & Structures WILEY

Railway wheelset fatigue life estimation based on field tests

Michele Maglio | **Elena Kabo** | **Anders Ekberg**

CHARMEC/Department of Mechanical and Maritime Sciences, Chalmers University of Technology, Gothenburg, Sweden

Correspondence
Michele Maglio, CHARMEC/Department of Mechanical and Maritime Sciences, Chalmers University of Technology, SE-412 96 Gothenburg, Sweden.
Email: michele.maglio@chalmers.se

Funding information
In2Track3

Abstract

Field tests using an instrumented powered wheelset were performed to investigate fatigue damage accumulation in railway axles. Axle bending strains were measured and post-processed to obtain axle stress spectra. Statistical analyses were used to investigate the variations of axle stress spectra due to changes in railway operation parameters. The study indicates that measured axle stress spectra can be modeled using truncated normal distributions, where the large majority of measured stress amplitudes are lower than 50 MPa. Stress cycles at higher amplitudes are affected by operation parameters such as track design, number of switches and crossings, and whether the wheelset is in a leading or trailing position. Variations in the obtained statistical distributions of axle stresses have been used as input for fatigue life analyses. It was concluded that fatigue damage can potentially initiate on axles suffering from corrosion or small surface cracks/scratches.

KEYWORDS

field measurements, railway axle fatigue life, railway wheelset maintenance, statistical analyses, stress spectra

1 | INTRODUCTION

Railway axles are critical components of a vehicle's running gear. Their correct functioning is essential for travel safety. Railway axle maintenance is regulated by the European Standard EN 15313.[1] According to this standard, non-destructive testing has to be performed on axles to detect possible cracks before those may reach a critical length, see Carboni.[2] Inspection intervals running gear are usually scheduled depending on the mileage covered by the vehicle. However, such a scheduling approach does not account for the operational conditions the wheelset has been subjected to and the resulting status of the railway wheelset. This results in risks of trains being put out of service to perform unnecessary maintenance, or wheelsets subjected to extreme loads potentially being maintained too late. For the train operator, this results in higher maintenance costs, lower fleet availability, and potential safety issues.

To avoid the downsides entailed in current inspection practices, train operators are currently aiming at optimizing their maintenance intervals according to the observed conditions of their assets, see Cantini et al.[3] This strategy is referred to as condition-based maintenance (Ben-Daya et al[4]), and it allows to postpone maintenance as long as the parameters used to monitor a certain asset fall in a "safe" range. This range can, for example, be prescribed by railway authorities or company practices, or determined by other forms of assessment. However, the fatigue design methods used in standards for railway axles vary significantly across the world, as shown by Makino et al.[5] Moreover, to facilitate the adoption of a

condition-based maintenance approach for railway axles, more knowledge regarding the statistical distribution of axle stress amplitudes is needed, as high stress amplitude values can have a negative influence on the axle fatigue life.

This gap has been partially filled by previous studies that investigated axle stress spectra. In Grubisic et al.,[6] the operational loading of wheelset axles has been represented by cumulative frequency distributions (spectra) of service stresses. The total spectrum is obtained by summing up the contributions from the service stresses measured for trains running over stretches, respectively, characterized by straight tracks, curved tracks, and by the presence of switches and crossings. A "synthetic design spectrum" was also obtained by fitting a normal distribution over numerically computed stress levels. In Maglio et al.,[7] bending stress spectra obtained by means of both numerical simulations and field tests have been used to assess the effects of wheel out-of-roundness (OOR) and rail roughness on the increase in axle stress magnitudes. It was shown that, for the studied cases, the increase in axle stresses due to rail roughness could overcome the increase in axle stress due to the degradation of the wheel tread geometry.

In other studies, measured or simulated axle stress spectra have used to perform fatigue analyses: in Wu et al.,[8] a spectrum made of five blocks aimed at representing the stress distribution in the axle under different operational conditions was used to estimate the effects of a decrease in fatigue limit due to foreign object damage on the axle. Wu et al.[9] used a stress spectrum to perform a stepwise fatigue assessment methodology where a safe life assessment step is followed by a damage tolerance analysis. In Nahlik et al.,[10] a load spectrum was obtained by dividing measured bending amplitudes in 36 blocks depending on the dynamic load coefficient (i.e., the ratio between static load and measured load). The spectrum was then used to estimate the residual lifetime of the axle depending on the presence of detected or undetected cracks based on linear elastic fracture mechanics as well as by accounting for the retardation effect due to the plastic zone at the crack tip. In Mädler et al.,[11] the residual lifetime of wheelset axles was estimated by carrying out an experiment with a test rig. The load history was derived from a load spectrum consisting of 17 block loads. In Beretta et al.,[12] stress spectra obtained from field measurements have been used in a probabilistic fatigue damage assessment to determine the risk of fatigue failure of high-speed and freight train axles during service. The load spectra, which represented different service conditions, were used in Monte Carlo analyses resulting in a safety factor for a target reliability against fatigue.

The investigations in the above-mentioned works were mainly focused on variations in residual fatigue lifetime based on pre-determined axle stress spectra. However, a remaining question is related to the effects of variations in operational conditions on such spectra. In the present investigation, stress spectra are not only obtained as the cumulative distribution of bending stress values throughout the whole duration of a field test. Instead, also the different contributions to the spectra given by the passage over some specific sections of the railway network are analyzed. These sections are chosen depending on some operational parameters such as speed limits, number of curves, switches, and crossings. This allows to account for the variations in measured stresses due to the different operational conditions that can occur during operations on a stretch of track.

In this work, data in terms of bending strains have been gathered using the instrumented telemetry system described in Maglio et al.[7] The system has been installed on a powered wheelset located at one end of a regional train. The train operates both on high-speed main railway lines (with a speed up to 200 km/h) as well as on single-track regional railways in Sweden. Stress spectra have been collected by the telemetry on-board computer unit between February 2019 and November 2020. More information about the field test is given in section 2 of the present work.

Axle bending stress spectra measured on different track sections have been used to estimate statistical distributions of axle stresses. Spectra obtained directly from field tests as well as spectra estimated from statistical distributions have been used as input to fatigue life analyses. In these analyses, different Wöhler (Stress-Number) curves were used to account for the influence of variations in axle surface conditions. Moreover, the reduction factors applied to the fatigue limits in the Wöhler curves have been compared to the effect of surface cracks of different lengths.

The obtained statistical distributions of axle stresses can be used to predict the stresses that have been experienced in service, thus allowing the train operator to adopt a predictive maintenance approach. Fatigue analyses may help in identifying threshold levels in axle surface conditions at which precautions need to be taken to avoid failures. Based on the results derived under different operational conditions, the planned maintenance can be scheduled to an earlier or later occasion, and priority can be given to wheelsets where the estimated residual fatigue lifetime is more critical. This would result in a more efficient use of resources for the train operator, as well as in more flexibility in the usage of the fleet.

2 | FIELD TEST

2.1 | The telemetry system

The telemetry system used in the field test monitoring stresses at a specified section of an axle was SmartSet®, developed by Lucchini RS. The telemetry system, which is described more in detail in Cantini et al.[3] and Maglio et al.,[7] consists of strain gauges and a telemetry module installed on the axle body, as well as of a data acquisition computer mounted on the vehicle body. In the present installation, two telemetry modules (each consisting of two full strain gauge bridges capable of measuring strains due to axle bending) are placed on the axle of a powered leading wheelset at a distance of 80 mm from the wheel seat, where the effect of the stress concentration is negligible. The telemetry module receives power from the train power supply via an induction power head that is installed on the gearbox frame. The power head generates an alternating current on the inductive coil that is installed on the axle and directly connected to the telemetry module. The locations of these components on the instrumented axle are indicated in Figure 1.

The telemetry module acquires data from the strain gauges and processes the signals according to a rain flow count algorithm. For each strain cycle identified by the algorithm, strain mean values and amplitudes are stored in matrices. Measured strains can then be easily converted into stresses. A Global System for Mobile Communications (GSM) antenna transfers matrices to a remote server when the train is at specific Global Positioning System (GPS) locations. This allows to relate measured stress spectra to traffic on specific sections of the network and thus to assess the influence of track quality on measured axle stresses.

The instrumented train is an electric multiple unit of type Coradia Duplex produced by Alstom and operated by the Swedish passenger train operator SJ. It consists of two or three double-decker coaches, and it can operate in both running directions at a maximum speed of 200 km/h. The axle load acting on the instrumented wheelset is around 18.25 tonnes. The end of the train where the instrumented wheelset is mounted is reserved for the driver and electric equipment. Consequently, the static load acting on the axle does not vary significantly during operation.

2.2 | Axle stress spectra

Measurement data collected by the telemetry system in the form of strain matrices have been converted into stress matrices. Data gathered while the instrumented wheelset was traveling between Gothenburg and Skövde are shown in Figure 2. To facilitate the comparison of measurements for stretches of different lengths, results have been normalized and plotted in terms of "cycle ratio." This ratio has been obtained by dividing the number of cycles falling within a stress amplitude bin with the total number of stress cycles measured during a given train ride. Moreover, cycles with measured stress amplitudes below 20 MPa have been removed from the plots as these are mainly due to oscillations in the voltage of the telemetry system.

In Figure 2A, stress amplitudes are compared for some measurements performed when the instrumented wheelset is in leading or in trailing position. As the train can travel in both directions and as the instrumented axle is located at one end of the train, the instrumented wheelset can either be the very first or the very last wheelset to negotiate curves and switches when the train is running. From Figure 2A, it is possible to notice that larger stress amplitudes (in the order of 70 MPa to 90 MPa) are registered when the instrumented wheelset is in leading position. This is due to the fact that the first wheelset in the train suffers from higher wheel–rail contact forces (see Andersson et al.),[13] which affects the measured stresses. As higher stresses can have much more

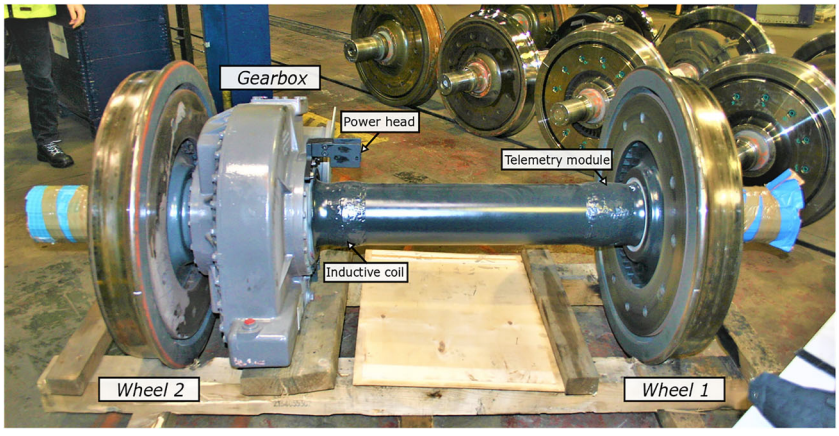

FIGURE 1 The instrumented wheelset with marked positions of the telemetry module, inductive coil, and power head before the installation under the train [Colour figure can be viewed at wileyonlinelibrary.com]

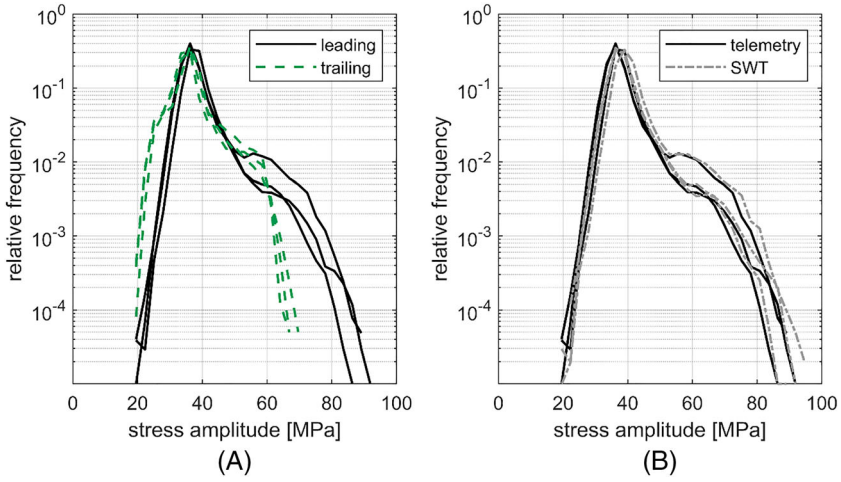

FIGURE 2 Relative frequency of occurrence of stress amplitudes obtained for the track section connecting Gothenburg to Skövde. Stress spectra are compared for (A) wheelset in leading or trailing position and (B) amplitudes as obtained from the telemetry or equivalent Smith-Watson-Topper (SWT) amplitudes for wheelset in leading position [Colour figure can be viewed at wileyonlinelibrary.com]

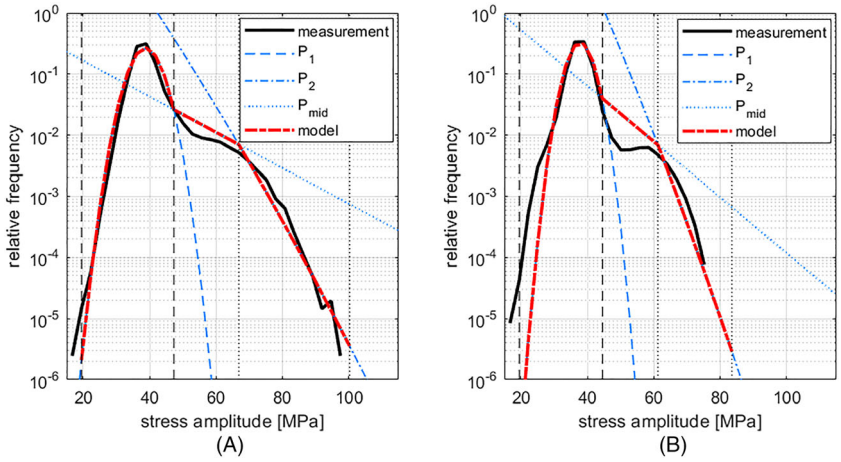

FIGURE 3 Relative frequency of occurrence of measured SWT equivalent stress amplitudes, the probability distributions P_1, P_2 and P_{mid}, and the resulting statistical model of the stress spectra obtained for the railway lines (A) Gothenburg–Skövde and (B) Skövde–Hallsberg. The black vertical dashed lines and the black vertical dotted lines indicate the stress intervals in which P_1 and P_2 are, respectively, used to determine the statistical model of stress spectra [Colour figure can be viewed at wileyonlinelibrary.com]

detrimental effects from a fatigue life perspective, the work presented in this paper will be based on measurements obtained when the instrumented wheelset is in the leading position.

As described in section 2.1, the strains measured by the telemetry strain gauges are stored in matrices based on combinations of strain amplitudes and their mean values. As the telemetry system mainly measures strains due to axle bending, most mean strain values are close to zero. As a consequence, once strains are converted into stresses, the mean stress for most cycles is close to zero. However, in order to properly account for the effect of mean stresses on the fatigue life of the axle, equivalent amplitudes according to the Smith-Watson-Topper (SWT) criterion are used in our analyses, see Dowling et al.[14] The SWT equivalent amplitude σ_{ar} for a stress cycle is computed as

$$\sigma_{ar} = \sqrt{\sigma_{max}\sigma_a} \ (\sigma_{max} > 0) \quad (1)$$

where σ_{max} and σ_a are, respectively, the maximum stress value and the stress amplitude registered for the same cycle. As the telemetry measurements are dominated by bending stresses and as mean stress values are relatively low, σ_{max} is always positive in our studies.

Figure 2B compares stress amplitudes (as obtained from the matrices) and equivalent SWT stress amplitudes for the three curves marked as "leading" in Figure 2A. It is possible to see that stress spectra consisting of SWT amplitudes are shifted about 1 to 2 MPa towards higher values. Although this increase in stresses is not expected to contribute significantly to the accumulation of fatigue damage in the axle, SWT equivalent amplitudes will be used in this work to properly account for the effect of mean stresses

2.3 | Statistical interpretation of stress spectra

Stress spectra obtained from different measurements performed between May 2019 and November 2020 for two different sections of the Swedish rail network (Gothenburg–Skövde and Skövde–Hallsberg) are plotted using thick dashed red lines in Figure 3A and 3B. During these measurements, the instrumented wheelset was

placed in leading position with respect to the train traveling direction. These track sections, which have comparable lengths, are part of "Västra Stambanan," a mixed traffic railway line connecting Gothenburg and Stockholm. Being part of the same line, the two sections are expected to undergo similar maintenance procedures and have similar levels of rail roughness.

From Figure 3, it can be noticed that the most frequently measured equivalent stress amplitudes fall between 35 MPa and 40 MPa, regardless of the route that the train is traveling on. This is expected as most of the equivalent stress amplitudes are only influenced by the (quasi-)static load acting on the axle, which depends on the weight of the train and not on the specific route. Moreover, Figure 3 shows that, as the equivalent stress amplitudes increase, their relative occurrence drops significantly, particularly for equivalent stress amplitudes larger than 60 MPa. It can be noted that the relative occurrence of equivalent stress amplitudes starts its rapid decrease at lower amplitude levels when the train is traveling on the route Skövde–Hallsberg (see Figure 3B) than on the route Gothenburg–Skövde (see Figure 3A). This cannot be explained by differences in track quality, as the two routes are expected to have similar speed limits and maintenance statuses. Instead, variations in relative occurrences of equivalent amplitudes may be due to differences in track design. These differences are summarized in Table 1, which shows the relative amounts of switches, crossings, and narrow curves on the two routes.

The amount of switches and crossings per kilometer for the route Skövde–Hallsberg is about 50% higher compared to the route Gothenburg–Skövde. Moreover, the occurrence of curves with radius lower than 1000 m of track is more than 10 times higher for the route Gothenburg–Skövde than for the route Skövde–Hallsberg. The route Gothenburg–Skövde is also characterized by a significant amount of sharp curves with radius lower than 700 m, which instead are not present on the Skövde–Hallsberg route. As switches and crossings as well as curves (and transitions curves) cause variations in the geometry of the track, leading to increased wheel–rail contact forces and axle stresses, they are likely reasons for the increased occurrence of higher equivalent stress amplitudes on the Gothenburg–Skövde route.

TABLE 1 Characteristics in terms of lengths and presence of switches, crossings, and curves of the railway lines Gothenburg–Skövde and Skövde–Hallsberg (source: Database BIS, Trafikverket)

Railway line	Gothenburg–Skövde	Skövde–Hallsberg
Length of the line (km)	143	109
Number of switches and crossings per km	0.59	0.39
Number of curves per km:		
with curve radius < 1000 m	0.43	0.04
with curve radius < 700 m	0.29	0

It should be pointed out that this investigation does not account for the variations in wheel OOR or rail roughness that have been observed during the measurement period. However, a study in Maglio et al.[7] has shown that the increase in axle bending stress amplitudes due to increased wheel OOR (up to 120 μm in peak-to-trough ovality) or due to a deterioration in rail surface roughness (up to 0.5 mm in peak-to-trough rail vertical roughness) is only in the order of a few megapascals. As a consequence, it is reasonable to expect that small variations in wheel OOR and rail roughness are not significant contributions to the variations in axle stress amplitude spectra.

Weather conditions and track stiffness were not monitored during the field test. However, as the measurements were performed over a period of 22 months, it can be expected that seasonal variations in weather and track stiffness are evened out throughout the different measurements for the same track section.

To obtain a model of the stress spectra that can be used to predict the wheelset loads during operations along a certain route, it is noted that the measured stress spectra are characterized by a peak in the interval between 35 MPa and 40 MPa and by a drop that generally occurs at stress levels higher than 60 MPa. In between, there is a section characterized by a slower decline or by a plateau in the frequency of measured stress levels.

Two normal distributions, denoted P_1 and P_2 in Figure 3, have been fitted to the first and last parts of each stress spectrum (each characterized, respectively, by a peak and by a drop in frequency of measured stress magnitudes). Consequently, the two normal distributions P_1 and P_2 are only fitted to the parts of the stress spectra located, respectively, to the left and to the right of the central plateau. The way the normal distributions P_1 and P_2 are fitted to the measured spectra is shown in Figure 4.

As seen in Figures 3 and 4, the two normal distributions deviate significantly from the measured curve (black solid line) towards the center of the spectra. In order to account for that, the distributions P_1 and P_2 have been truncated before the difference in relative frequency between the measured stress spectra and the statistical distributions reaches 50%. The SWT stress amplitude value at which the difference between P_1 and P_2 and the measured spectra exceeds this threshold is shown in

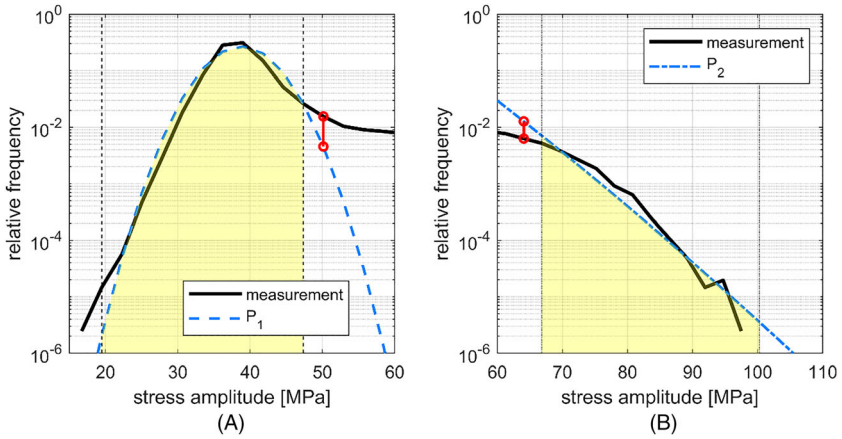

FIGURE 4 Fitted probability distributions (A) P_1 and (B) P_2 over the stress spectrum obtained for the railway line Gothenburg–Skövde. The area highlighted in yellow is the part of these probability distributions that is used in the statistical model of the stress spectrum [Colour figure can be viewed at wileyonlinelibrary.com]

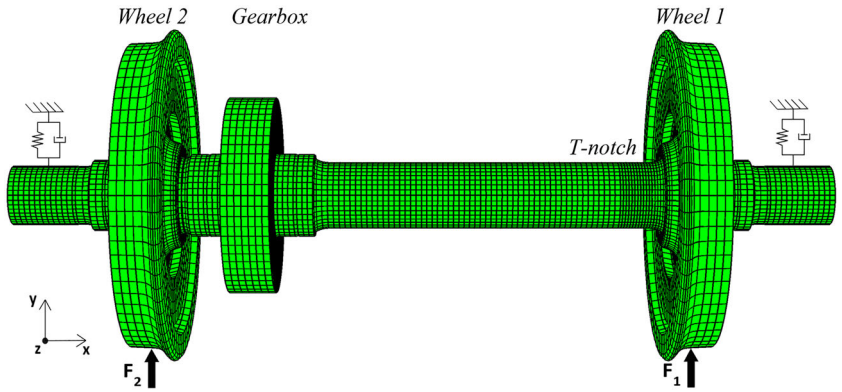

FIGURE 5 FE model of instrumented wheelset that was used to estimate the stress concentration factor K_t at the axle fillet radius below wheel 1 [Colour figure can be viewed at wileyonlinelibrary.com]

Figure 4 with red vertical segments ending with circles. As stress spectra are stored by the telemetry in stress bins which are 2.8 MPa wide, the truncation occurs at the bin closest to the one where the threshold is exceeded. After the truncation procedure has occurred, only the untruncated parts of normal distributions P_1 and P_2 (highlighted in yellow in Figure 4) are used to model the load spectra.

In Figure 3, the stress amplitude levels at which P_1 and P_2 have been truncated are marked with black vertical dashed lines and black vertical dotted lines, respectively. The part of the stress spectra located between the two truncated normal distributions (roughly corresponding to stress amplitudes between 45 MPa and 60 MPa) has been modeled by a straight line in the semi-logarithmic diagrams and is denoted P_{mid}. The truncated distributions P_1, P_{mid}, and P_2 form the full stress spectra model. In Figure 3, it is indicated by dashed red lines.

The obtained models of stress spectra can be useful in the design of wheelset components as well as in maintenance planning, as service loads in real operations are often higher than the ones that can be determined according to the procedures suggested in the standards such as EN 13013–1,[15] see Grubisic et al.[6]

3 | FATIGUE ANALYSES

Both the stress spectra obtained from the measurements and those obtained from the statistical models can be used to predict the residual lifetime of the wheelset. The analyses performed in this work will be focused on axle fatigue, but the method can be applied to other wheelset components by transforming to relevant service stresses.

In the present field test, stress amplitudes have been derived by measuring axle strains in a location where the effects of stress concentrations are not present. However, stresses will increase towards the fillet radius located below the wheel seat, also known as T-notch, where axles are most commonly cracked, see Lundén et al.[16] and Madia et al.[17] To account for the state of stress in the vicinity of the T-notch, a three-dimensional finite element (FE) model of the instrumented wheelset was used, see Figure 5. The model has 788,568 degrees of freedom and is loaded with two unit forces F_1 and F_2 applied on the nominal circles of the two wheels and acting along the vertical direction. The vertical displacement of the wheelset is limited by the primary suspension, which is modeled as two pairs of springs and dampers. The springs stiffness is 2 MN/m, and the dampers viscous coefficient

is 20 kNs/m. The material properties and the geometry of the model are described in detail in Maglio et al.[18] A static analysis showed that the maximum bending stress value at the T-notch is 1.26 times higher than at the cross section of the axle where the strain gauges are mounted. As a consequence, a static stress concentration factor $K_t = 1.26$ has been used in the present work for the T-notch.

3.1 | Fatigue life relationship

In order to assess the fatigue life of the axle under different operational conditions, reduction factors to be applied to the Wöhler curve (S–N curve) were estimated from test data and modified according to the method of Juvinall et al.[19] as described in Dowling et al.[20]

The axle of the instrumented wheelset is made of EA1N steel. According to the European Standard EN 13261,[21] the ultimate tensile strength (σ_U) of that material falls in the range between 550 MPa and 650 MPa. In the present study, $\sigma_U = 600$ MPa has been used. Fatigue limits for axles made of EA1N steel were obtained from full-scale tests in Cervello.[22] For such an axle with a surface roughness in the range 0.8 to 1.6 Ra (presuming to correspond to a machined surface), an average fatigue limit of 248 MPa (with a standard deviation of 34 MPa) was estimated for 10^7 stress cycles. This corresponds to a fatigue limit of 181 MPa for 2.5% probability of failure. Calculations in this study are performed for axles in service and are therefore mainly aimed for maintenance planning. Therefore, the average fatigue limit is used, as it gives a more realistic estimation of the residual life of the axle. The fatigue limit for 2.5% probability of failure should be used when designing the axle, as a larger safety margin should be aimed for.

According to Juvinall's method, the reduced fatigue limit of the Wöhler curve for steels σ_{er} is obtained as

$$\sigma_{er} = m \cdot \sigma_U \tag{2}$$

where m is defined as

$$m = m_e m_t m_d m_s \tag{3}$$

In equation 3, $m_e = 0.5$ is a standard reduction factor used for steels with $\sigma_U < 1400$ MPa, m_t accounts for the type of loading acting on the axle, m_d is the size factor accounting for the diameter of the axle, and m_s accounts for the surface status of the axle and depends on the material σ_U. As the full-scale fatigue test in Cervello[22] accounted for the size of the axle as well as for the type of loading (bending), the only reduction factor from equation 3 which was applied in the present study is m_s. The latter has been varied to estimate the influence of axle surface conditions which differ from the one of the full-scale tests (machined axle), see section 3.2.

To account for the reduction in fatigue life due to the stress concentration at the T-notch, the previously obtained Wöhler curve has been additionally reduced by the factor k_f. This factor is obtained from the stress intensity factor k_t, the fillet radius ρ, and the UTS σ_U by using the approach from Peterson,[23] see equation 4:

$$k_f = 1 + q(k_t - 1) \tag{4}$$

where

$$q = \frac{1}{1 + \frac{\alpha}{\rho}} \tag{5}$$

$$\log\alpha = 2.654 \cdot 10^{-7}\sigma_U^2 - 1.309 \cdot 10^{-3}\sigma_U + 0.01103 \tag{6}$$

with σ_u in MPa, which gives $k_f = 1.256$.

According to Juvinall's theory, the Wöhler curve can be expressed as a straight line in a semilogarithmic stress-cycles chart between the fatigue limit, $\frac{\sigma_{er}}{k_f}$, and the stress amplitude $0.9 \cdot \frac{\sigma_U}{k_f}$ corresponding to a fatigue life of 1000 cycles. To match the experimental data in Cervello,[22] the fatigue limit was set at 10^7 cycles.

Fatigue life analyses have been performed for the T-notch using as input both the stress spectra obtained from the measurements and those obtained from the fitted statistical distributions. In this paper, results obtained for the stretches Gothenburg–Skövde and Skövde–Hallsberg are presented, but the approach has also been applied to analyze other stretches of the Swedish railway network.

In our analyses, three different fatigue damage calculation algorithms have been applied. In the first one, it is assumed that stress cycles whose equivalent SWT amplitudes fall below $\frac{\sigma_{er}}{k_f}$ (i.e., the reduced fatigue limit for 10^7 cycles) do not cause any fatigue damage. This is the least conservative design approach. In the second approach, it is assumed that all cycles cause the same amount of fatigue damage that would be predicted by simply prolonging the slope of the S–N curve for fatigue lives higher than 10^7 cycles. This is the most conservative approach and may result in an over-conservative design and fatigue life estimations. In the third approach, it is assumed that the Wöhler curve continues after 10^7 cycles with a reduced slope (one third the slope of the S–N curve between 10^3 and 10^7 cycles). The Wöhler curves resulting from these assumptions are sketched in Figure 6.

The damage accumulated after each stress cycle has been estimated using the procedure described by Palmgren.[24] The total fatigue damage D caused by a series of i stress amplitudes where each stress amplitude is applied N_i times and corresponds to $N_{f,i}$ cycles to failure is computed as

$$D = \sum_i \frac{N_i}{N_{f,i}} \tag{7}$$

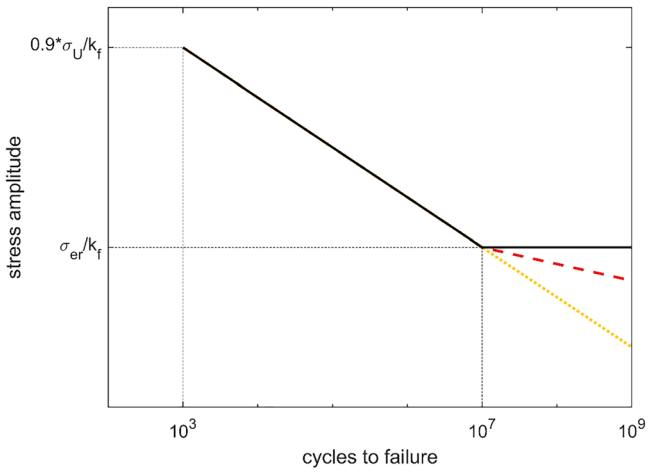

FIGURE 6 Wöhler curves for the following assumptions on the fatigue limit: stress amplitudes below the fatigue limit do not generate any fatigue damage (solid black line), the slope of the S–N curve is reduced to one third of the original one after the fatigue limit (dashed red line), and the slope of the S–N curve is not changed (dotted light orange line) [Colour figure can be viewed at wileyonlinelibrary.com]

Fatigue failure is presumed to occur when $D = 1$.

3.2 | Effect of operational conditions

The Wöhler curves represented in Figure 6 have been adopted to estimate axle fatigue life using the stress spectra (with SWT correction) obtained from the telemetry measurements as well as the spectra obtained from the statistical models. When analyses are based on the statistical distributions, a Monte Carlo approach is used. Here, stress amplitudes are not extracted from measured spectra but derived from random realizations of the model distribution built up from the truncated distributions P_1, P_{mid}, and P_2 according to their pertinent (truncated) probability density functions. Realizations are allocated to one of the three truncated distributions depending on their cumulative probability. This implies that, for example, more realizations are generated based on P_1 than P_2. Each realization in the Monte Carlo approach corresponds to a SWT stress amplitude value.

In order to account for a large variety of possible maintenance conditions, in particular relating to the axle surface conditions, different values for the surface roughness coefficient m_s have been applied when reducing the Wöhler curve. The magnitude of m_s affects the fatigue limits for 10^7 cycles as shown by dotted gray vertical lines in Figure 7.

Figure 7 shows that the estimated axle fatigue life is strongly dependent on the reduction factors applied to the Wöhler curve as well as on the adopted fatigue life algorithm. In contrast, despite the two railway stretches

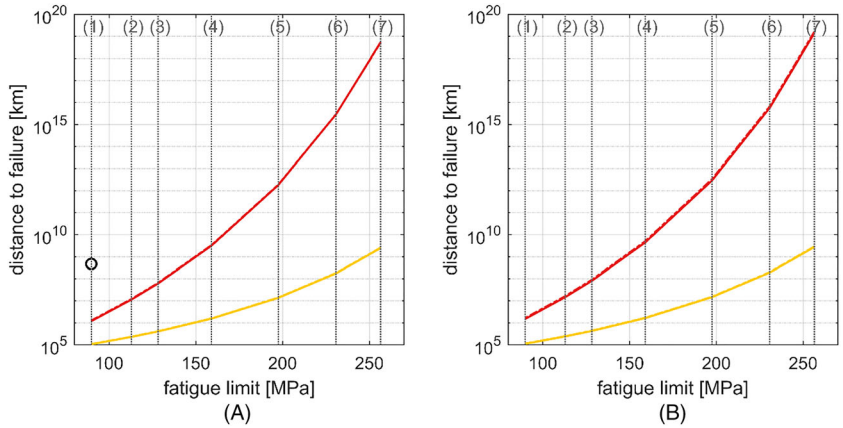

FIGURE 7 Estimated distance to failure depending on the assumed fatigue limit for 10^7 cycles for the stretches (A) Gothenburg–Skövde and (B) Skövde–Hallsberg. The black circle indicates distance to failure presuming no fatigue damage generated at stress magnitudes below the fatigue limit. Red and yellow curves are based on the assumption that the Wöhler curve continues after 10^7 cycles with one third of the original slope and an unchanged slope, respectively. The solid lines correspond to the statistical representation of the stress spectra, and the dotted ones to spectra from telemetry measurements (as illustrated in Table 2). Fatigue limits correspond to axle surface conditions: (1) corroded in salt water, (2) as forged, (3) corroded in tap water, (4) hot rolled, (5) machined, (6) fine ground, and (7) mirror polished [Colour figure can be viewed at wileyonlinelibrary.com]

generating different axle stress spectra, no large differences are visible between Figure 7A and 7B. This is due to the fact that the largest majority of stress cycles correspond to the part of the stress spectra represented by the probability distribution P_1 which does not differ significantly between the two running cases. Even if the equivalent stress amplitudes modeled by P_1 are relatively low in magnitude, their relative frequency is so high that they contribute for the largest share of the total damage D (see equation 7) when it is assumed that all stress cycles contribute to the accumulation of fatigue damage (i.e., in the cases represented by the red and yellow curves in Figure 7). The black circle shows that, if it is assumed that stress amplitudes below the fatigue limit are presumed not to generate any fatigue damage, fatigue failure can only occur for axles with very critical surface conditions. This hypothesis is non-conservative and unrealistic, and should not be adopted for maintenance planning.

Moreover, it can be concluded that there are no large differences in predicted fatigue lives between measured and simulated stress spectra. This indicates that approximating stress spectra using statistical distributions leads to a low error, see the following section.

3.3 | Sensitivity analyses

As Figure 7 is plotted in semi-logarithmic scale, it might be difficult to notice small variations between the different curves. Table 2 has been added to clarify the differences in expected axle fatigue lives between the two stretches as well as between the two modeling assumptions for stress spectra. In the results shown in Table 2, the axle surface is assumed to be fine ground, and the Monte Carlo analyses have been performed with 10^7 trials.

Table 2 confirms that the statistically derived stress spectra introduce differences in estimated distances to axle failures lower than 15% and in many cases lower than 5%. It can be noticed that the differences in expected axle fatigue life between the two track sections are strongly dependent on the hypotheses on the slope of the Wöhler curve (i.e., on whether the slope is reduced or not after 10^7 cycles). Indeed, if it is assumed that the slope of the Wöhler curve does not change, the expected axle life differs about 8% between the two stretches, while it differs of over 40% if the S–N curve slope is reduced to one third after 10^7 cycles. This is due to the fact that in the

TABLE 2 Expected travel distance to axle failure. The results correspond to a presumption of an S–N curve with a constant slope or a one third slope at stress amplitudes below the nominal fatigue limit

	Expected distance to axle failure (km)		Difference in expected distance to failure between models	
Model for stress spectra based on	**Same S–N slope**	**1/3 slope**	**Same S–N slope**	**1/3 slope**
Gothenburg–Skövde				
Telemetry	$49*10^8$	$65*10^{13}$	4.1%	3.1%
Monte Carlo	$47*10^8$	$63*10^{13}$		
Skövde–Hallsberg				
Telemetry	$53*10^8$	$117*10^{13}$	3.7%	14.4%
Monte Carlo	$51*10^8$	$102*10^{13}$		

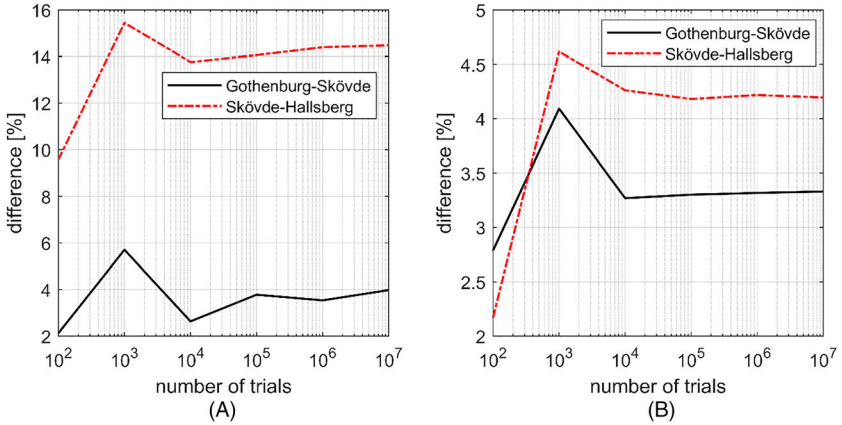

FIGURE 8 Difference in expected axle fatigue life computed using the stress spectra from the strain gauges or the statistical models of stress spectra. Calculations have been made using Wöhler curves where the slope (A) is reduced to one third after 10^7 cycles, and (B) does not change [Colour figure can be viewed at wileyonlinelibrary.com]

latter case stress cycles with lower amplitudes generate a lower amount of fatigue damage. Thus, less fatigue damage is accumulated for a stretch where registered stress amplitudes are lower (such as Skövde–Hallsberg).

Monte Carlo analyses whose results in terms of fatigue life are shown in Figure 7 have been performed for 10^7 trials. However, it is possible to obtain robust results even with significantly lower amounts of trials. Figure 8 shows the difference in expected axle fatigue life computed using the stress history from the telemetry or the Monte Carlo approach as a function of the amount of trials.

Figure 8 shows that the error obtained using the Monte Carlo method tends to stabilize after some 10^4 to 10^5 trials. This means that reliable fatigue life analyses can be made with a low computational cost (a Monte Carlo fatigue analysis with 10^6 trials and accounting for the three different fatigue algorithms requires around 3 min to be performed on an Intel i7 processor).

3.4 | Effect of overloads

The stress spectra and the statistical distributions in Figure 3 show that a clear majority of cycles are characterized by stress amplitudes lower than 50 MPa. The occurrence of those stresses is modeled by the statistical distribution P_1, see section 2.3. Moreover, the results from fatigue life analyses summarized in Table 2 and discussed in section 3.2 indicate that cycles with lower stress amplitudes actually generate the largest contribution to fatigue damage—how large this contribution is depends on the assumptions made on the slope of the Wöhler curve, see section 3.1.

The share of fatigue damage caused by the three statistical distributions P_1, P_2, and P_{mid} (see Figure 3) in the fatigue life analyses performed with the Monte Carlo method is shown in Table 3. The analyses are related to the stretches Gothenburg–Skövde and Skövde–Hallsberg. The axle surface was supposed to be machined, a condition that corresponds to the vertical lines marked with (5) in Figure 7.

It can be noticed that stress cycles with relatively low amplitudes (i.e., those modeled by the distribution P_1) account for between 39% and 82% of the accumulated damage depending on track quality and assumptions on the fatigue algorithm. Stress amplitudes falling under the distribution P_2 can reasonably be classified as overloads. From Table 3, it can be noticed that overloads can significantly affect the fatigue life of the axle if the slope of the Wöhler curve is reduced after 10^7 cycles, since 11% to 27% of the fatigue damage is generated by these loads. If the slope of the S–N curve is instead presumed to be unaffected by the fatigue limit, overloads only account for 2% to 4% of the fatigue damage. In this more conservative approach, indeed, stress cycles at lower amplitudes generate more fatigue damage.

To investigate this topic more in depth, fatigue life analyses featuring only stress cycles from the

	Constant S–N slope			1/3 slope after 10^7 cycles		
Railway lines	P_1	P_{mid}	P_2	P_1	P_{mid}	P_2
Gothenburg–Skövde	79.2%	17.1%	3.7%	39.3%	34.1%	26.9%
Skövde–Hallsberg	81.2%	16.9%	2.0%	54.4%	34.6%	11.0%

TABLE 3 Share of fatigue damage generated by stresses belonging to the three statistical distributions. Monte Carlo analyses with 10^7 trials under two different assumptions for the Wöhler curve (constant slope of the S–N curve, and a slope reduced to one third of the original one after 10^7 cycles)

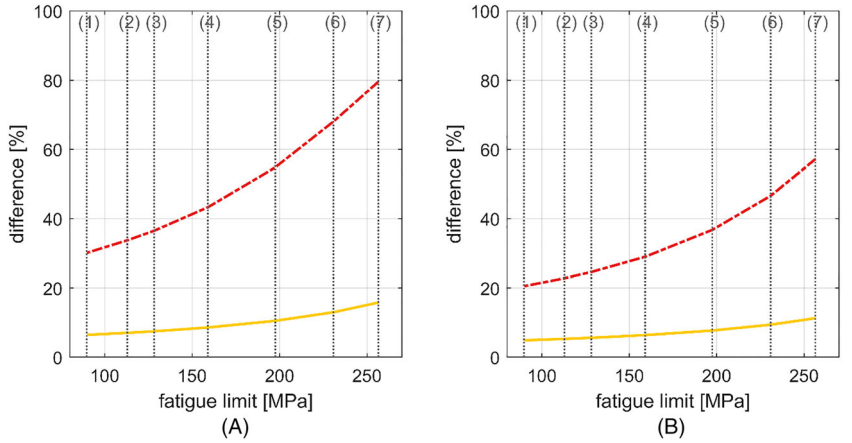

FIGURE 9 Difference in expected axle fatigue life depending on whether the three distributions P_1, P_{mid}, and P_2 or only untruncated P_1 are accounted for in the analysis. Calculations have been made using Wöhler curves where the slope is reduced to one third after 10^7 cycles (dashed-dotted red lines) or with a constant slope (solid yellow lines). Simulations are referred to the stretches (A) Gothenburg–Skövde and (B) Skövde–Hallsberg. Fatigue limits are indicated using the same style as in Figure 7 [Colour figure can be viewed at wileyonlinelibrary.com]

untruncated normal distribution P_1 as input in the Monte Carlo analyses have been performed. The difference between the expected axle fatigue lives including the three distributions P_1, P_{mid}, and P_2 and the fatigue analysis featuring the untruncated P_1 distribution is plotted as a function of the axle surface conditions in Figure 9, and fatigue limits as in Figure 7. The Monte Carlo analyses have been performed with 10^7 trials and are related to the stretches Gothenburg–Skövde and Skövde–Hallsberg. The percentages of Figure 9 are based on the expected fatigue life if all three distributions are accounted for.

Figure 9 shows that cycles with higher stress levels are less significant if the slope of the S–N curve is not changed. This is, as also remarked above, due to the fact that stress cycles at lower amplitudes generate more fatigue damage if the slope of the S–N curve is unchanged.

Not accounting for the probability distributions P_{mid} and P_2 leads to a larger overestimation of the fatigue life for the stretch Gothenburg–Skövde than for Skövde–Hallsberg. This is due to the generally higher stress levels on the first stretch. Overall, under the assumption that the slope of the Wöhler curve is reduced after 10^7 cycles, neglecting cycles with higher stress levels leads to a large overestimation of the fatigue life (between 20% and 80%).

3.5 | Effect of small surface cracks

Axle structural integrity is reduced by the presence of small surface defects (cracks) that may not be detected during scheduled inspections. In Beretta et al.,[25] the effect of corrosion by rainwater on the S–N diagram of A1N steel was studied by means of fatigue tests on cylindrical specimens.

A link between the size of a surface defect (for example, a crack) and the reduction of the fatigue limit can also be found using small crack theory. In Murakami et al.,[26] the projected area $\sqrt{A}$ (in μm) of a small surface defect (where $\sqrt{A} < 1{,}000\,\mu m$) was found to correspond to the reduced fatigue limit in rotating bending σ_{er} (in MPa) of a material component with Vickers hardness H_V (in kgf/mm^2) of

$$\sigma_{er} = \frac{1.43 \cdot (H_V + 120)}{(\sqrt{A})^{1/6}} \tag{8}$$

Note that the dimensions in empirical expression 8 are not consistent. The constants in 8 are independent on the material. They were determined by Murakami and Endo by the least square method applied to experimental data as described in Murakami et al.[27] For a semi-circular crack of radius a, where $= \frac{\pi a^2}{2}$, expression 8 can be written as

$$a = \left[\frac{0.138 \cdot (H_V + 120)}{\sigma_{er}}\right]^6 \tag{9}$$

where a (μm), σ_{er} (MPa), H_V (kgf/mm^2). Expressions 8 and 9 are valid in the small crack region, that is, when the reduced fatigue limit σ_{er} computed according to

$$\sigma_{er} = 0.138 \cdot (H_V + 120) \cdot a^{-1/6} \tag{10}$$

is below the unreduced fatigue limit σ_e. If the relation $H_V = \frac{\sigma_u}{3.2}$ (in kgf/mm^2) from Murakami[28] is employed (where σ_u is the ultimate tensile strength in MPa), σ_e (in MPa) can be estimated as

$$\sigma_e \approx 1.6 \cdot H_V = 0.5 \cdot \sigma_u \tag{11}$$

Moreover, expressions 8 and 9 are valid below the threshold stress for crack growth σ_{LEFM} which can be computed according to linear elastic fracture mechanics (i.e., large crack theory) as in Dowling et al.[29]:

$$\sigma_{LEFM} = \frac{\Delta K_{th}}{2F\sqrt{\pi a}} \tag{12}$$

where ΔK_{th} is the threshold stress intensity factor for crack growth. For a small semi-circular crack, it is reasonable to assume a crack geometry factor $F = 0.73$, see Dowling et al.[29]

In El Haddad et al.,[30] the threshold stress intensity factor for crack growth is linked to the effective crack length $(a + l_0)$ by the following expression, where l_0 is a constant for a given material:

$$\Delta K_{th} = \Delta S\sqrt{\pi(a + l_0)} \tag{13}$$

As the stress range ΔS corresponds to twice the stress amplitude, expression 13 can be reformulated in terms of a reduced fatigue limit σ_{er}, where $\Delta S = 2 \cdot \sigma_{er}$, as

$$\sigma_{er} = \frac{\Delta K_{th}}{2\sqrt{\pi(a + l_0)}} \tag{14}$$

According to El Haddad et al.,[30] the crack length at the unreduced fatigue limit σ_e corresponds to l_0. This yields

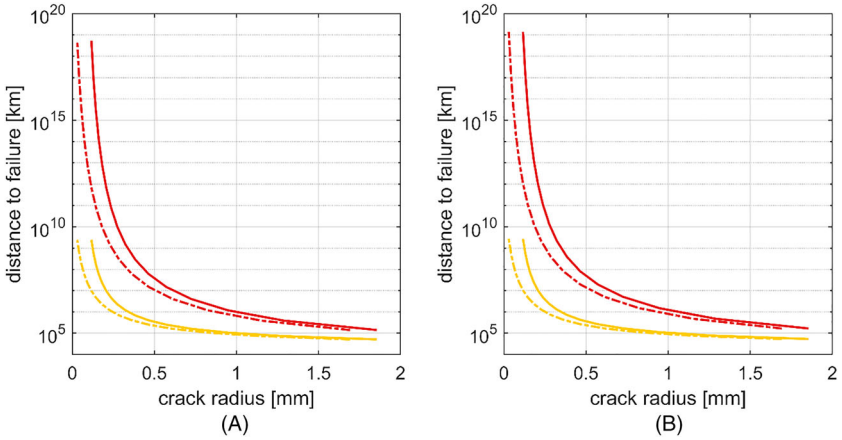

FIGURE 10 Expected axle fatigue life as a function of the length of a small semi-circular surface crack according to Murakami's theory (solid lines) or El Haddad's theory (dashed-dotted lines). Calculations have been made using Wöhler curves with the slope is reduced to one third of the original one after 10^7 cycles (red lines) or with constant slope (yellow lines). Simulations are referred to the stretches (A) Gothenburg–Skövde and (B) Skövde–Hallsberg [Colour figure can be viewed at wileyonlinelibrary.com]

$$\Delta K_{th} = 2F\sigma_e\sqrt{\pi l_0} \tag{15}$$

$F = 1$ can be presumed for a small crack in fatigue limit testing. Introducing expression 15 in expression 14 yields

$$\sigma_{er} = \frac{\sigma_e\sqrt{l_0}}{\sqrt{a + l_0}} \tag{16}$$

By assuming $F = 0.73$, $\Delta K_{th} = 7$ MPa $\cdot$ m$^{1/2}$ (according to Dowling et al.[31]), and $\sigma_e = 1.6 \cdot H_V$ as in 11, expression 15 gives the value of l_0 (in meters) as

$$l_0 = \frac{1}{\pi}\left(\frac{\Delta K_{th}}{1.46 \cdot \sigma_e}\right)^2 \approx \frac{2.86}{H_V^2} \tag{17}$$

Using l_0 from expression 17 and $\sigma_e = 1.6 \cdot H_V$ into expression 16 gives

$$\sigma_{er} = \frac{\sqrt{\frac{2.86}{H_V^2}}}{\sqrt{a + \frac{2.86}{H_V^2}}} \cdot 1.6 \cdot H_V = \frac{2.7}{\sqrt{a + \frac{2.86}{H_V^2}}} \tag{18}$$

which allows to express the crack radius a (in meters) as

$$a = \left(\frac{2.7}{\sigma_{er}}\right)^2 - \frac{2.86}{H_V^2} \tag{19}$$

Equations (9) and (19 have been used to obtain the radii of small semi-circular surface cracks that would generate different reduced fatigue limits σ_{er} for the axle. Then, axle residual lives for the two stretches Gothenburg–Skövde and Skövde–Hallsberg have been computed for the above-mentioned reduced fatigue limits and for different assumptions on the slope of the Wöhler curve. Estimated fatigue lives for axles affected by small semi-circular surface cracks were thus obtained according to the theories of Murakami and El Haddad, see Figure 10. These analyses do not account for the variation in stress intensity factors due to crack growth, and the adopted equations are only valid for small cracks. As a consequence, results are only indicative and intended to be used as an aid in maintenance planning.

Figure 10 shows a good match between the results obtained with Murakami and El Haddad theories. Again, the expected fatigue life changes significantly depending on the assumptions made on the slope of the Wöhler curve and on the adopted fatigue algorithm.

4 | CONCLUDING REMARKS

Bending stress spectra of railway axles have been derived from field tests. A method to obtain statistical descriptions of these spectra using truncated normal distributions has been presented. Field test and statistical stress spectra have been used as input to fatigue life analyses accounting for different assumptions on the Wöhler curve. Results show a good agreement between fatigue lives obtained from measured and statistically described stress spectra. Moreover, it was shown that Monte Carlo-based fatigue life predictions converge after a relatively low amount of trials. Results in terms of expected fatigue lives are heavily dependent on the hypotheses made on the reduction of the Wöhler curve at lives >10^7.

The derived statistical stress amplitude distribution provides an objective categorization of the track section quality with respect to wheelset loading. The developed fatigue assessment approach can also be used to predict the estimated residual fatigue lifetime of wheelset components, contributing to the adoption of a condition-based maintenance approach. In future work,

efforts will be made to link the parameters of the statistical distributions used to model stress spectra with measured track conditions (e.g., track geometry deviations, amount of transition curves, and of switches and crossings).

ACKNOWLEDGMENTS

The current work is part of the activities within the Centre of Excellence CHARMEC (CHAlmers Railway MEChanics, www.chalmers.se/charmec). Parts of the study have been funded from the European Union's Horizon 2020 research and innovation program in the project In2Track3 under grant agreement No. 101012456.

DATA AVAILABILITY STATEMENT

Research data are not shared.

NOMENCLATURE

A	projected area of surface defect
a	crack length
D	accumulated fatigue damage
F	crack geometry factor
H_V	Vickers hardness
K	crack stress intensity factor
k	notch stress intensity factor
m	S–N curve reduction factor
N	number of stress cycles to failure
P	probability distribution
σ_a	stress amplitude
σ_{ar}	Smith-Watson-Topper (SWT) equivalent stress amplitude
σ_{er}	reduced fatigue limit for rotating bending
σ_{LEFM}	threshold stress for crack growth
σ_{max}	maximum stress value
σ_u	ultimate tensile strength

ORCID

Michele Maglio https://orcid.org/0000-0001-7881-7617
Anders Ekberg https://orcid.org/0000-0002-3219-1855

REFERENCES

1. European committee for standardization (CEN). *Railway Applications - In-Service Wheelset Operation Requirements - In-Service and Off-Vehicle Wheelset Maintenance*. Brussels: CEN; 2017 Standard No. EN 15313:2016; 118 pp.
2. Carboni M. Reliability of non-destructive testing in the railway field: common practice and new trends. In: Prabhakar VV, Raghu VP, Narendra SJ, eds. *Risk Based Technologies*. Singapore: Springer; 2019:173-191.
3. Cantini S, Cervello S, Regazzi D, Corbizi Fattori A, Labbadia L. Optimization of in-service UT inspection intervals based on wheelset loads monitoring—SMARTSET®. In: *Proceedings of the XIX International Wheelset Congress (IWC2019); 2019 June 16–20; Venice, Italy* 6 pp.
4. Ben-Daya M, Kumar U, Prabhakar Murthy DN. Chapter 16, Condition-based maintenance. In: *Introduction to Maintenance Engineering: Modeling, Optimization and Management*. New York (USA): John Wiley & Sons Ltd; 2016:355-387.
5. Makino T, Kato T, Hirakawa K. Review of the fatigue damage tolerance of high-speed railway axles in Japan. *Eng Fract Mech*. 2011;78(5):810-825.
6. Grubisic V, Fischer G. Procedure for reliable durability validation of train axles. *Mater Sci Eng Technol*. 2006;37:973-982.
7. Maglio M, Vernersson T, Nielsen JCO, et al. Railway wheel tread damage and axle bending stress—instrumented wheelset measurements and numerical simulations. *Int J Rail Transport*. 2021;10(3):23-297.
8. Wu SC, Xu ZW, Kang GZ, He WF. Probabilistic fatigue assessment for high-speed railway axles due to foreign object damages. *Int J Fatigue*. 2018;117:90-100.
9. Wu SC, Liu YX, Li CH, Kang GZ, Liang SL. On the fatigue performance and residual life of intercity railway axles with inside axle boxes. *Eng Fract Mech*. 2018;197:176-191.
10. Náhlík L, Pokorný P, Ševčík M, Fajkoš R, Matušek P, Hutař P. Fatigue lifetime estimation of railway axles. *Eng Failure Anal*. 2017;73:139-157.
11. Mädler K, Geburtig T, Ullrich D. An experimental approach to determining the residual lifetimes of wheelset axles on a full-scale wheel-rail roller test rig. *Int J Fatigue*. 2016;86:58-63.
12. Beretta S, Regazzi D. Probabilistic fatigue assessment for railway axles and derivation of a simple format for damage calculations. *Int J Fatigue*. 2016;86:13-23.
13. Andersson E, Berg M, Stichel S. Chapter 13, Examples on vehicle-track interaction. In: *Rail Vehicle Dynamics*. Stockholm (Sweden): Railway Group KTH; 2014 18 pp (and 6 pp appendix).
14. Dowling NE, Kampe SL, Kral ML. Chapter 9, Fatigue of Materials: Introduction and Stress-Based Approach. In: *Mechanical Behavior of Materials*. 5th ed. Harlow (UK): Pearson Education Ltd; 2020:375-449.
15. European Committee for Standardization (CEN). *Railway Applications—Wheelsets and Bogies—Part 1: Design method for axles with external journals*. Brussels: CEN; 2017 Standard No. EN 13103–1:2017; 14 pp.
16. Lundén R, Vernersson T, Ekberg A. Railway axle design: to be based on fatigue initiation or crack propagation? *Proc Inst Mech Eng F*. 2010;224(5):445-453.
17. Madia M, Beretta S, Schödel M, Zerbst U, Luke M, Varfolomeev I. Stress intensity factor solutions for cracks in railway axles. *Eng Fract Mech*. 2011;78(5):764-792.
18. Maglio M, Pieringer A, Nielsen JCO, Vernersson T. Wheel–rail impact loads and axle bending stress simulated for generic distributions and shapes of discrete wheel tread damage. *J Sound Vib*. 2021;502: 19 pp.
19. Juvinall RC, Marshek KM. *Fundamentals of Machine Component Design*. 5thed. Hoboken, New Jersey (USA): John Wiley; 2012.
20. Dowling NE, Kampe SL, Kral ML. Chapter 10, Stress-Based approach to Fatigue: Notched Members. In: *Mechanical Behavior of Materials*. 5th ed. Harlow (UK): Pearson Education Ltd; 2020:450-516.

21. European committee for standardization (CEN). *Railway Applications - Wheelsets and Bogies - Axles - Product Requirements*. Brussels: CEN; 2020 Standard No. EN 13261:2020; 74 pp.
22. Cervello S. Fatigue properties of railway axles: new results of full-scale specimens from Euraxles project. *Int J Fatigue*. 2016; 86:2-12.
23. Peterson RE. *Stress Concentration Factors*. New York (USA): John Wiley; 1974. 336 pp.
24. Palmgren A. Die Lebensdauer von Kugellagern (*Life span of Ball Bearings* – in German). *Zeltschrift Des Vereines Deutscher Ingenieure (J Assoc German Eng)*. 1923;68:339-341.
25. Beretta S, Carboni M, Fiore G, Lo Conte A. Corrosion– atigue of A1N railway axle steel exposed to rainwater. *Int J Fatigue*. 2010;32(6):952-961.
26. Murakami Y, Endo M. Effects of defects, inclusions and inhomogeneities on fatigue strength. *Int J Fatigue*. 1994;16(3): 163-182.
27. Murakami Y, Endo M. Effect of hardness and crack geometries. In: Miller KJ, de los Rios ER, eds. *The Behaviour of Short Fatigue Cracks*. London: Mechanical engineering Publications Ltd; 1986:275-293.
28. Murakami Y. Chapter 5, Effect of hardness H_v on fatigue limits of materials containing defects, and fatigue limit prediction equations. In: *Metal fatigue: effects of small defects and nonmetallic inclusions*. 2nd ed. Oxford (UK): Academic Press; 2019:61-94.
29. Dowling NE, Kampe SL, Kral ML. Chapter 8, Fracture of Cracked Members. In: *Mechanical Behavior of Materials*. 5th ed. Harlow (UK): Pearson Education Ltd; 2020:294-374.
30. El Haddad MH, Smith KN, Topper TH. Fatigue crack propagation of small cracks. *J Eng MaterTechnol*. 1979;101:42-46.
31. Dowling NE, Kampe SL, Kral ML. Chapter 8, Fracture of Cracked Members. In: *Mechanical Behavior of Materials*. 4th ed. Harlow (UK): Pearson Education Ltd; 2013:334-415.

How to cite this article: Maglio M, Kabo E, Ekberg A. Railway wheelset fatigue life estimation based on field tests. *Fatigue Fract Eng Mater Struct*. 2022;1-14. doi:10.1111/ffe.13756